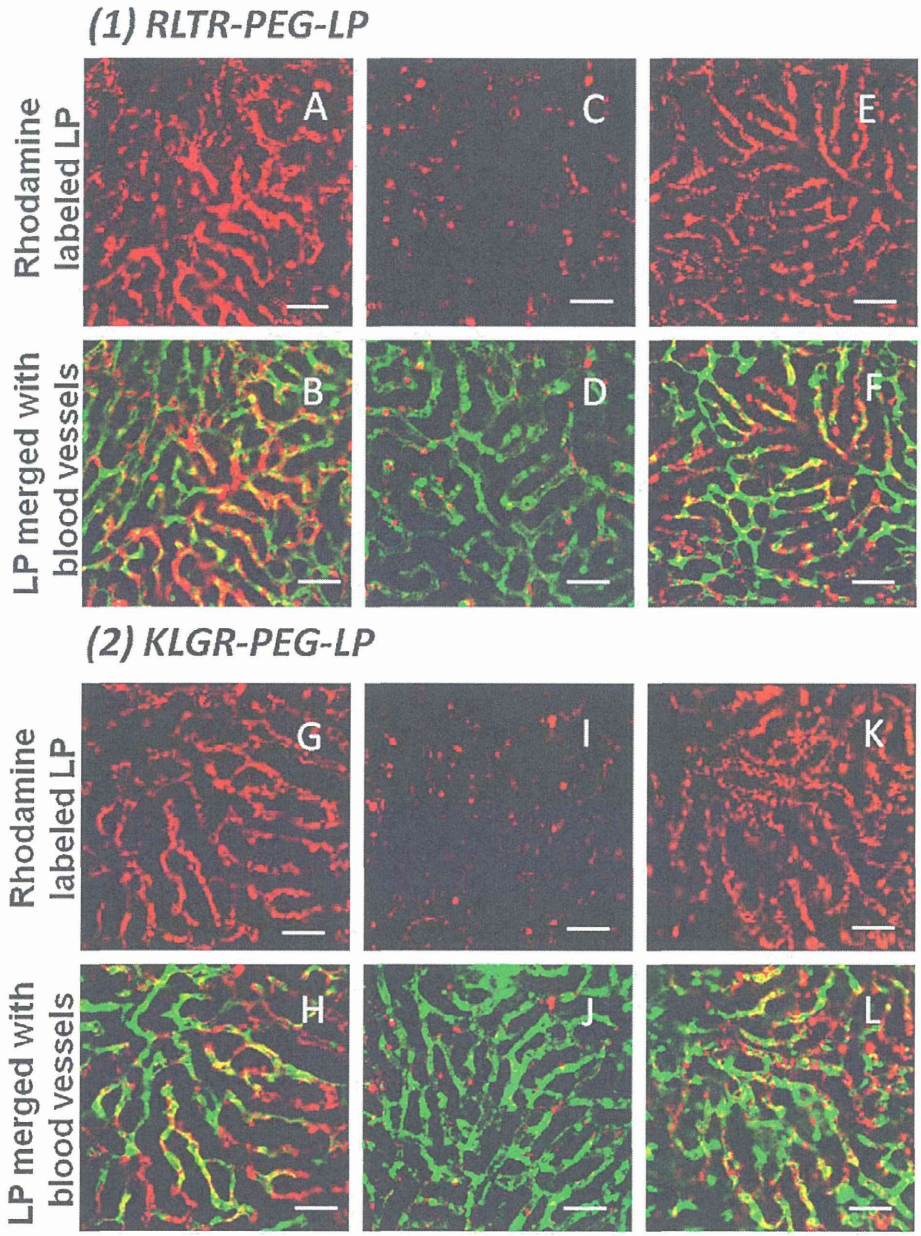

Fig. 4. In vivo competitive inhibition studies of RLTR-PEG-LPs or KLGR-PEG-LPs using unlabeled RLTR-PEG-LPs or KLGR-PEG-LPs or cationic LPs. Green and red color represents blood vessels stained by Isolectin B4 and rhodamine labeled LPs respectively. Mice were pretreated with unlabeled RLTR-PEG-LPs or KLGR-PEG-LPs or cationic LPs 15 min before the second treatment with labeled RLTR-PEG-LPs or KLGR-PEG-LPs for another 25 min of incubation. Representative images of liver tissues with (A and B) labeled RLTR-PEG-LPs, (C and D) labeled RLTR-PEG-LPs pre-treated with unlabeled RLTR-PEG-LPs, (E and F) labeled RLTR-PEG-LPs pre-treated with unlabeled cationic LPs, (G and H) labeled KLGR-PEG-LPs, (I and J) labeled KLGR-PEG-LPs pre-treated with unlabeled KLGR-PEG-LPs, (K and L) labeled KLGR-PEG-LPs pre-treated with unlabeled cationic LPs are shown. Scale bars correspond to 50 μm in all images.

LPs was quite different from that of the RLTR-PEG-LPs, in which the cationic LPs were gathered in particular spots (Fig. 3D). In addition, these dots did not overlap with liver endothelial cells (Fig. 3E and F) indicating that they were taken up by non-parenchymal cells such as Kupffer cells or were merely aggregated LPs.

3.4. In vivo inhibition study

In order to examine some possible mechanisms of unique targeting ability of RLTR peptide into liver endothelial cells, comparative studies of RLTR and its reversed peptide sequence named as KLGR were performed in the following part. Both RLTR-PEG-LPs and KLGR-PEG-LPs were accumulated along with the liver blood vessels (Fig. 4A and B, G and H). Next, accumulation of both labeled RLTR-PEG-LPs and KLGR-PEG-LP along with the liver blood vessels were dramatically inhibited by a pre-treatment with unlabeled RLTR-PEG-LPs or KLGR-PEG-LPs (Fig. 4C and D, I and J), however, small portions of signal were remaining. In contrast, the accumulation of both labeled RLTR-PEG-LPs or KLGR-PEG-LP was not reduced by the pre-treatment with unlabeled cationic LPs (Fig. 4E and F, K and L). The results generated in this study suggest that cationic charge is not the reason for this uptake and may be both RLTR peptide and its reverse sequence, the KLGR peptide has some specificity for liver endothelial cells. Possible interpretations will be discussed in Section 4.

3.5. In vitro comparative inhibition study of RLTR-PEG-LPs

This experiment was performed to support the in vivo inhibition data. We compared the cellular uptake of both RLTR-PEG-LPs and

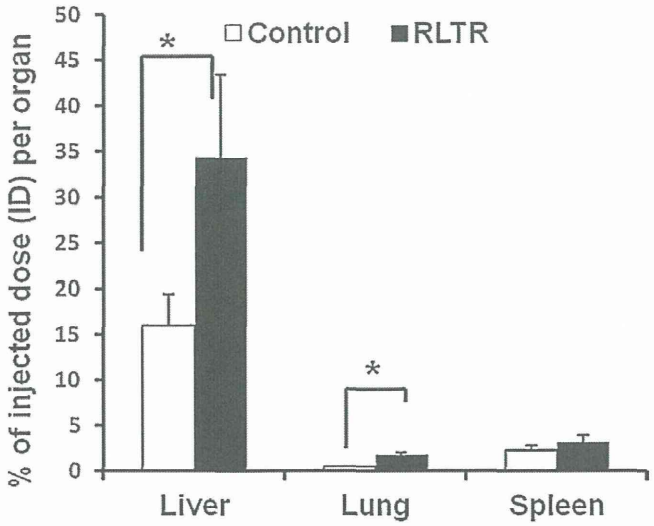

Fig. 2. Biodistribution of ^{3}H-CHE labeled RLTR-PEG-LPs and LPs in different organ. Male ICR mice were intravenously injected with labeled RLTR-PEG-LPs and LPs. After 25 min of incubation different organs of mouse were collected and radioactivity was measured. Tissue accumulation of LPs was represented as % of injected dose (ID). Here, % of ID is expressed as the mean ± SD (n = 4). Statistical analyses were performed by the unpaired Student's t-test, where $^{*}P < 0.05$.

3. Results

3.1. Synthesis of RLTR-PEG-DSPE

The thiol group of the cystein residue in the RLTR peptide was conjugated by reaction with Mal-PEG$_{2000}$-DSPE at 37 °C for 24 h (Reaction scheme is shown in the supplementary figure 1). MALDI-TOF MS analyses confirmed the synthesis of RLTR-PEG-DSPE.

Supplementary material related to this article can be found, in the online version, at http://dx.doi.org/10.1016/j.ijpharm.2013.07.068.

3.2. The characteristic of RLTR-PEG-LPs and its cellular uptake

The selected RLTR peptide was attached to the top of PEG in PEGylated liposomes. PEG liposomes (PEG-LPs) and RLTR modified PEG liposomes (RLTR-PEG-LPs) were prepared by incorporating PEG-DSPE or RLTR-PEG-DSPE at levels of 1, 3, 5, or 10 mol% of the total lipid. The physical properties of the prepared LPs are shown in Table 1. To evaluate the effect of the RLTR peptide on cellular uptake, we next examined the cellular uptake of RLTR-PEG-LPs and PEG-LPs in primary liver endothelial cells (LECs) and in Hepa1-6 cell line. The RLTR peptide enhanced the cellular uptake of PEG-LPs and the maximum cellular uptake was observed within 3 mol% of RLTR peptide modification in both the cells (Fig. 1A and B).

3.3. In vivo selectivity of RLTR peptide

A biodistribution study of RLTR-PEG-LPs was carried out in order to confirm the targeting ability of RLTR-PEG modified LP. Compared to unmodified control LPs, RLTR-PEG-LPs were largely accumulated in the liver, with only negligible accumulation in the lung or spleen, within a very short time (Fig. 2). The liver targeting ability of RLTR peptide was more than its ability to target lung or spleen. We then obtained an in vivo image of the liver to check the distribution pattern of this RLTR-PEG modified LP in liver.

We then performed an in vivo accumulation study to verify our hypothesis outlined in the introduction part. We investigated the intrahepatic distribution of RLTR-PEG-LPs by confocal microscopy. Rhodamine-labeled RLTR-PEG-LPs were widely distributed throughout the blood vessels (Fig. 3A), and these intensities were essentially merged with the signal for Isolectin B4, a marker of endothelial cells (Fig. 3B and C). These results demonstrate that RLTR-PEG-LPs efficiently target liver endothelial cells rather than hepatocytes. Furthermore, we compared the intrahepatic distribution pattern with RLTR-PEG-LPs and cationic LPs in order to evaluate the effect of the cationic charge of the liposomal surface. The size and zeta-potential of the rhodamine-labeled RLTR-PEG-LPs and cationic LPs was 125 nm, 26 mV and 132 nm, 22 mV respectively. The intrahepatic distribution pattern of the cationic

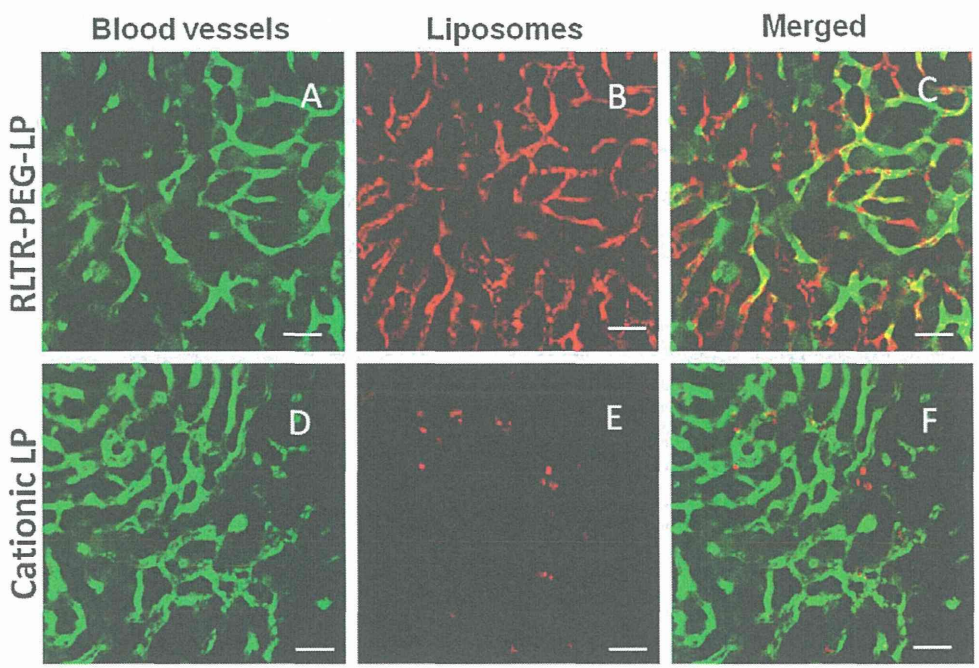

Fig. 3. Representative intrahepatic distribution pattern of RLTR-PEG-LPs (A–C) and a cationic control LPs, in which the lipid composition was DC6-14/DOPE/Chol = 4:3:3 (D–F). Green and red color represents blood vessels stained by Isolectin B4 and rhodamine labeled LPs respectively. Scale bars correspond to 50 μm in all images.

tors, the peptide modified PEG-LP is highly accumulated in liver EC. It is possible that this carrier system has more specificity for liver EC, rather than hepatocytes. This surprising accumulation of this carrier system through blood vessels led us to conclude that this nanoparticle might be an ideal system for targeting the liver endothelial cells. The finding that cationic peptides and lipids accumulate at high levels in endothelial cells of liver is attractive and interesting. There are very few reports of the use of cationic or neutral nano carriers to target liver endothelial cells (Bartsch et al., 2004; Toriyabe et al., 2011). It should be noted that, these systems failed to achieve high accumulation in liver endothelial cells. Because of this, in this study we seized the opportunity to develop this nanocarrier to target liver EC. There are two possible reasons for the high accumulation of RLTR modified PEG-LP in liver EC. Either the high cationic charge of the peptide is causing this high accumulation or the peptide sequence itself has specificity for liver endothelial cell. We then checked the specificity of both RLTR and its reverse sequence KLGR modified PEG-LP by both an in vitro and in vivo inhibition study. In the in vivo inhibition study we demonstrated that both the RLTR-PEG-LPs and KLGR-PEG-LPs uptake were inhibited by unlabeled RLTR-PEG-LPs and KLGR-PEG-LPs respectively (Fig. 4). However, the cationic LPs did not affect its uptake both in vivo or in vitro (Figs. 4 and 5). Given these findings, the possibility of a higher accumulation in LEC is due to a higher cationic charge can be excluded. We then attempted to address the second possible reason of the higher accumulation in LEC, namely, the sequence of the peptide. We found that the sequence contain a motif RKR which remains the same both in the RLTR and KLGR peptide, although the sequence is completely reversed. It has been reported that stearylated polyarginine and its derivatives, i.e. stearyl-$(RXR)_4$ mediates the efficient plasmid transfection in several cell lines (Lehto et al., 2010). The RKR motif is similar as the RXR motif (Fig. 6). As our study shows that both the RLTR (RLT**RKR**GLK) and KLGR (KLG**RKR**TLR) modified PEG-LP are equally efficient in targeting LEC, the possibility that the RKR sequence is responsible for this targeting cannot be completely excluded. There is another possibility, i.e. both peptides contain an RXXR motif. According to CendR theory this RXXR sequence is essential for a tissue penetrating property (Teesalu et al., 2009). As our peptide sequence RLTR (**RLTR**KRGLK) and KLGR (**KLGR**KRTLR) both have the RXXR sequence and supporting CendR theory so there is another possibility that **RLTR** and **KLGR** are the true motifs for these two peptides for targeting LEC (Fig. 6). Both the peptide, RLTR and KTLR, modified LPs appear to have similar targeting abilities for liver EC. However, we were not able to identify the receptor or the key motif responsible for this targeting. Further study will be required to identify the motif or the receptor. LDL receptor, LRP-1, RXR or RXXR motif, which are mentioned in the introduction and discussion, are all possibilities.

5. Conclusion

Liposomes modified with the peptide sequence RLTRKRGLK or its reverse sequence KLGRKRTLR, designed based on the ApoB-100 sequence, accumulated at high levels in liver endothelial cells via some as-yet-unidentified target receptors, and not via non-specific binding with the cell surface. The presence of RXR or RXXR motif in both peptides may explain their similar uptake by liver ECs. The RLTR or KLGR modified liposomes have the potential for use as a carrier system for the delivery of drugs to liver endothelial cells.

Acknowledgements

This study was supported by grants from the Special Education and Research Expenses of the Ministry of Education, Culture, Sports, Science and Technology of Japan. The authors also wish to thank Dr. Milton S. Feather for his helpful advice in writing the English manuscript.

References

Akino, T., Hida, K., Hida, Y., Tsuchiya, K., Freedman, D., Muraki, C., 2009. Cytogenetic abnormalities of tumor-associated endothelial cells in human malignant tumors. Am. J. Pathol. 75, 2657–2667.

Bartsch, M., Weeke-Klimp, A.H., Hoenselaar, E.P., Stuart, M.C., Meijer, D.K., Scherphof, G.L., Kamps, J.A., 2004. Stabilized lipid coated lipoplexes for the delivery of antisense oligonucleotides to liver endothelial cells in vitro and in vivo. J. Drug Target. 12, 613–621.

Brown, M.S., Deuel, T.F., Basu, S.K., Goldstein, J.L., 1978. Inhibition of binding of low density lipoprotein to its cell surface receptors in human fibroblasts by positively charged proteins. J. Supramol. Struct. 8, 223–234.

Dominique, T., Vijay, S., 2010. Intrahepatic angiogenesis and sinusoidal remodeling in chronic liver disease: new targets for the treatment of portal hypertension? J. Hepatol. 53, 976–980.

Du, S.L., Pan, H., Lu, W.Y., Wang, J.W., Wang, J.Y., 2007. Cyclic Arg-Gly-Asp peptide labeled liposomes for targeting drug therapy of hepatic fibrosis in rats. J. Pharmacol. Exp. Ther. 322, 560–568.

Hatakeyama, H., Akita, H., Maruyama, K., Suhara, T., Harashima, H., 2004. Factors governing the in vivo tissue uptake of transferring-coupled polyethylene glycol liposomes in vivo. Int. J. Pharm. 281, 25–33.

Hida, K., Hida, Y., Amin, D.N., Flint, A.F., Panigrahy, D., Mortonet, C.C., 2004. Tumor-associated endothelial cells with cytogenetic abnormalities. Cancer Res. 64, 8249–8255.

Ishiwata, H., Suzuki, N., Ando, S., Kikuchia, H., Kitagawa, T., 2000. Characteristics and biodistribution of cationic liposomes and their DNA complexes. J. Control. Release 69, 139–148.

Kibria, G., Hatakeyama, H., Harashima, H., 2011. A new peptide motif present in the protective antigen of anthrax toxin exerts its efficiency on the cellular uptake of liposomes and applications for a dual-ligand system. Int. J. Pharm. 412, 106–114.

Kmieč, Z., 2001. Cooperation of liver cells in health and disease. Adv. Anat. Embryol. Cell Biol. 161, 1–151.

Lehto, T., Abes, R., Oskolkov, N., Suhorutšenko, J., Copolovici, D.M., 2010. Delivery of nucleic acids with a stearylated (RxR)4 peptide using a non-covalent co-incubation strategy. J. Control. Release 141, 42–51.

Marit, S.N., Rune, B., Christian, A.D., Grete, M.K., Kaare, R.N., Trond, N.B., 1998. Uptake of LDL in parenchymal and non-parenchymal rabbit liver cells in vivo. Biochem. J. 254, 443–448.

Ohga, N., Hida, K., Hida, Y., Muraki, C., Tsuchiya, K., Matsuda, K., 2009. Inhibitory effects of epigallocatechin-3 gallate, a polyphenol in green tea, on tumor-associated endothelial cells and endothelial progenitor cells. Cancer Sci. 100, 1963–1970.

Oie, C.I., Appa, R.S., Hilden, I., Petersen, I., Gruhler, H.H., Smedsrød, A.B., 2011. Rat liver sinusoidal endothelial cells (LSECs) express functional low density lipoprotein receptor related protein-1 (LRP-1). J. Hepatol. 55, 1346–1352.

Puri, A., Loomis, K., Smith, B., Lee, J., Yavlovich, H., Heldman, A.E., 2009. Lipid-based nanoparticles as pharmaceutical drug carriers: from concepts to clinic. Crit. Rev. Ther. Drug Carrier Syst. 26, 523–580.

Ramadori, G., Moriconi, F., Malik, I., Dudas, J., 2008. Physiology and pathophysiology of liver inflammation, damage and repair. J. Physiol. Pharmacol. 59, 107–117.

Rajkumar, C., Gerene, M.D., Gee, W.L., Michael, C.G., Sarah, N.H., David, G., Le, C., 2010. Pathogenesis of the hyperlipidemia of Gram-negative bacterial sepsis may involve pathomorphological changes in liver sinusoidal endothelial cells. Int. J. Infect. Dis. 14, e857–e867.

Teesalu, T., Sugahara, K.N., Kotamraju, V.R., Ruoslahti, E., 2009. C-end rule peptides mediate neuropilin-1-dependent cell, vascular, and tissue penetration. Proc. Natl. Acad. Sci. U.S.A. 106, 16157–16162.

Thomas, E.W., Anders, N., Joachim, H., 1999. Lipoprotein receptors: new roles for ancient proteins. Nat. Cell Biol. 1, 157–162.

Toriyabe, N., Hayashi, Y., Hyodo, M., Harashima, H., 2011. Synthesis and evaluation of stearylated hyaluronic acid for the active delivery of liposomes to liver endothelial cells. Biol. Pharm. Bull. 34, 1084–1089.

Urban, O., German, C., Goran, B., 1993. Binding of a synthetic apolipoprotein B-100 peptide and peptide analogues to chondroitin 6-sulfate: effects of the lipid environment. Biochemistry 32, 1858–1865.

Urban, O., German, C., Eva, H., Karin, C., Goran, E.B., 1997. Possible functional interactions of apolipoprotein B-100 segments that associate with cell proteoglycans and the ApoB/E receptor. Arterioscler. Thromb. Vasc. Biol. 17, 149–152.

Biomaterials 34 (2013) 5617–5627

Contents lists available at SciVerse ScienceDirect

Biomaterials

journal homepage: www.elsevier.com/locate/biomaterials

The effect of liposomal size on the targeted delivery of doxorubicin to Integrin αvβ3-expressing tumor endothelial cells

Golam Kibria [a], Hiroto Hatakeyama [a], Noritaka Ohga [b], Kyoko Hida [b], Hideyoshi Harashima [a,*]

[a] Laboratory of Innovative Nanomedicine, Faculty of Pharmaceutical Sciences, Hokkaido University, Kita 12, Nishi 6, Kita-ku, Sapporo, Hokkaido 060-0812, Japan
[b] Division of Vascular Biology, Graduate School of Dental Medicine, Hokkaido University, Kita 13, Nishi 7, Kita-ku, Sapporo, 060-8586, Japan

ARTICLE INFO

Article history:
Received 31 January 2013
Accepted 29 March 2013
Available online 24 April 2013

Keywords:
Size of liposomes
Ligand multivalency
Drug-resistant cancer
Tumor vasculature targeting
Anti-angiogenic effect

ABSTRACT

Size of the liposomes (LPs) specially governs its biodistribution. In this study, LPs were developed with controlled sizes, where variation in LP size dictates the ligand–receptor interaction, cellular internalization and its distribution within the tumor microenvironment. The therapeutic efficacies of doxorubicin (DOX)-loaded RGD modified small size (~100 nm in diameter, dnm) and large size (~300 dnm) PEGylated LPs (RGD-PEG-LPs) were compared to that of Doxil (a clinically used DOX-loaded PEG-LP, ~100 dnm) in DOX resistant OSRC-2 (Renal cell carcinoma, RCC) tumor xenografts. Doxil, which accumulated in tumor tissue via the enhanced permeability and retention (EPR) effect, failed to suppress tumor growth. Small size RGD-PEG-LP, that targets the tumor endothelial cells (TECs) and extravasates to tumor cells, failed to provide anti-tumor effect. Large size RGD-PEG-LP preferentially targets the TECs via minimization of the EPR effect, and significantly reduced the tumor growth, which was exerted through its strong anti-angiogenic activity on the tumor vasculature rather than having a direct effect on DOX resistant RCC. The prepared large size RGD-PEG-LP that targets the TECs via interacting with Integrin αvβ3, is a potentially effective and alternate therapeutic strategy for the treatment of DOX resistant tumor cells by utilizing DOX, in cases where Doxil is ineffective.

1. Introduction

Liposomes (LPs) have been extensively studied as drug delivery systems. The size of a LP is a major determinant of its biodistribution as well as the systemic stability. Small size PEGylated LPs (PEG-LPs) of around 100 nm in diameter (dnm) are widely used to target many diseased tissues including cancer [1–4]. Doxil, a typical successful example of doxorubicin (DOX) loaded small size PEG-LP (~100 dnm), functions against the tumor cells via the enhanced permeability and retention (EPR) effect [3,4]; and when modified with specific ligands, has been used previously to target the tumor vasculature [5–7]. In previous studies, the interaction of PEG-LP modified with CD13 with NGR was used to target the vasculature of GI-LI-N, HTLA-230 and IMR-32 neuroblastoma tumors [5], where the IC50 values for these cells to DOX were found to be 0.4 μM, 0.6 μM and 0.02 μM, respectively [8,9]. Later, the recognition of Integrin αvβ3 by RGD modified PEG-LP was used to target the vasculature of an SN12C renal cell carcinoma (RCC) [6]; where the EC50 value of the SN12C cells to DOX was found to be 50 ng/ml [10]. Additionally, NG2 Proteoglycan interacting TAASGVRSMH/LTLRWVGLMS [11], a membrane type-1 matrix metalloproteinase (MT1-MMP) interacting GPLPLR [12] and the APRPG ligand (the target receptor is unknown at present) [13] modified PEG-LPs were used to target the vasculatures of melanoma (B16F10), Colon 26 NL-17 and glioblastoma tumors, respectively. It should be noted that the compatibility of the selected target molecules and the specific ligand is an important issue in terms of exerting the pharmacological effect of the nanoparticles against a tumor type.

The endothelial cell gaps in the tumor vasculature are much higher (~100–600 nm) [14] than that of the normal endothelium (<6 nm) [15]; therefore, it is much easier for small size PEG-LPs (60–150 dnm) to extravasate to tumor cells [2,4], a process called the EPR effect. On the other hand, large size particles (>200 dnm) more promptly adhere to the target cells by facilitating ligand–receptor interactions [16–18], despite their limitations related to their recognition by reticuloendothelial system

* Corresponding author. Tel.: +81 11 706 3919; fax: +81 11 706 4879.
E-mail address: harasima@pharm.hokudai.ac.jp (H. Harashima).

0142-9612/$ – see front matter © 2013 Elsevier Ltd. All rights reserved.
http://dx.doi.org/10.1016/j.biomaterials.2013.03.094

(RES) as well as being entrapped in splenic sinusoidal filters [19–21]. Therefore, we hypothesized that large size PEG-LP would be more effective in terms of targeting diseased tissues once they were modified with a specific ligand. In this study, we prepared small size (~100 dnm) and large size (~300 dnm) PEG-LPs modified with RGD ligand (RGD-PEG-LPs). The effect of the size of PEG-LPs on cellular internalization, ligand–receptor interactions as well as on *in vitro* drug delivery efficiency was evaluated using human umbilical vein endothelial cells (HUVEC) that express Integrin αvβ3 [22]. To observe the tissue distribution as well as the therapeutic effect, size controlled PEG-LPs were applied to mice bearing kidney cancer (human RCC), which is notoriously resistant to chemotherapy [23–27], where various multidrug-resistant proteins are responsible for drug resistance. Because of this, it would be difficult to treat RCC by delivering a drug to tumor cells. In tumor tissue, vascular endothelial cells (TECs) play a critical role in tumor growth and progression by providing nutrients, oxygen, growth factors etc. to tumor cells [7,28,29]. The frequent mutation of the von Hippel-Lindau (VHL) protein triggers the up-regulation of vascular endothelial growth factor (VEGF) production and results in the progression of highly angiogenic RCC tumors [30]. Sunitinib, Sorafenib and Bevacizumab have been approved for the treatment of RCC which function against VEGF and VEGF receptors (VEGFRs) [31,32], suggesting the effectiveness of anti-angiogenic therapy against RCC. However, RCC can become resistant to these drugs [33–35], which also have a number of side effects, including cardiac toxicity, hepatotoxicity, hypothyroidism, anemia, hand-foot syndrome etc [36]. Therefore, as an alternate approach, a drug delivery system that targets the tumor vasculature would be necessary for RCC tumor therapy.

For targeting the vasculature in OSRC-2 (RCC) tumor tissue, we recently developed a large size PEG-LP (~300 dnm) modified with two different types of ligands ((CD13 specific ligand NGR; and a non-specific cell penetrating peptide, tetra-arginine (R4)) which exhibited better anti-tumor effect, as NGR alone showed poor therapeutic efficacy [37]. While the NGR motif exerts its efficiency in other tumor types [5], its activity with respect to RCC is poor. The findings of the present study indicate that large size PEG-LP, modified only with a single ligand RGD (RGD-PEG-LP) which interacts with Integrin αvβ3, is efficient to both targeting and disrupting the tumor vasculature in OSRC-2 tumor tissue. Additionally, we provide more evidences and a mathematical explanation for the therapeutic efficacy of large size RGD-PEG-LP over the small size versions against the RCC tumor model.

To overcome the limitations associated with the drug resistance of RCC as well as considering the side effects of on-going therapy; we proposed an active targeting liposomal delivery system aimed at treating RCC by delivering DOX to TECs via targeting the Integrin αvβ3 receptor. We prepared DOX loaded small size (~100 dnm) and large size (~300 dnm) RGD-PEG-LPs and their anti-tumor activity was investigated and compared with Doxil in mice bearing human RCC (OSRC-2) tumors.

2. Materials and methods

2.1. Materials

Hydrogenated soybean phosphatidylcholine (HSPC), Egg phosphatidylcholine (EPC), Cholesterol, N-(lissamine rhodamine B sulfonyl)-1,2-dioleoyl-sn-glycero-3-phosphoethanolamine (rhodamine-DOPE), 1,2-distearoyl-sn-glycero-3-phosphoethanolamine-N-[methoxy(polyethyleneglycol)-2000] (PEG-DSPE) were purchased from Avanti Polar Lipids (Alabaster, AL, USA). cRGDfK peptide was purchased from Peptides International, Inc. (Louisville, KY, USA) and conjugated with PEG-DSPE as reported before [22]. Doxorubicin Hydrochloride was purchased from Wako Pure Chemical Industries (Osaka, Japan). ^{3}H-Cholesteryl hexadecyl ether (^{3}H-CHE) was purchased from PerkinElmer Life Science (MA, USA). RPMI 1640 were purchased from Sigma (St. Louis, MO, USA). EGM-2 and EGM-2 MV medium were purchased from Lonza (Walkersville, MD, USA).

2.2. Isolation of mouse tumor endothelial cells (TECs)

OSRC-2 tumor endothelial cells (OSRC-EC) were isolated as described previously [38–40]. Briefly, TECs were isolated from OSRC-2 tumors and dermal tissue in tumor-bearing mice using a magnetic cell sorting system (MACS; Milteny Biotec). TECs were plated onto 1.5% gelatin-coated culture plates and grown in EGM-2 MV (Clonetics) and 15% fetal bovine serum (FBS). Diphtheria toxin (500 ng/ml; Calbiochem) was added to TEC subcultures to kill any remaining human tumor cells.

2.3. Cell lines and culture

Human renal cell carcinoma (RCC), OSRC-2 cells (Riken Cell Bank, Tsukuba, Japan) were cultured in RPMI 1640 supplemented with heat-inactivated 10% FBS and penicillin (100 units/ml), streptomycin (100 μg/ml) under an atmosphere of 5% CO_2 at 37 °C, and used within 6 months of purchasing. OSRC-EC and Human umbilical vein endothelial cells (HUVEC) were cultured in EGM-2 MV and EGM-2 medium, respectively.

2.4. Animal experiments

BALB/cAJcl-nu/nu male mice (CLEA, Japan), 4 weeks of age were allowed to food and water under controlled environmental conditions. Animal experiments were performed according to the national regulations and approved by the Hokkaido University Animal Care Committee.

2.5. Preparation of PEG-LPs

2.5.1. Preparation of PEG-LPs for in vitro cellular uptake

LPs composed of EPC and Cholesterol (molar ratio: 7/3) were prepared by the lipid film hydration method. After evaporation under nitrogen gas, dried lipid films were hydrated with phosphate buffer saline (PBS, pH 7.4), followed by vortexing. During film formation, 1.5 mol% rhodamine-DOPE was incorporated to label the lipid composition. To prepare large size particles, the prepared LPs were extruded through a 0.4 μm polycarbonate filter. To prepare small size particles, the dried lipid films were hydrated with PBS (pH 7.4) followed by sonication in a bath-type sonicator (AU-25C, Aiwa, Japan). The prepared LPs were extruded through a 0.08 μm polycarbonate filter to control the size. After extrusion, the total lipid concentration in LPs was determined. LPs were incubated with 5 mol% PEG-DSPE or RGD-PEG-DSPE at 60 °C for 30 min to prepare PEG-LP or RGD-PEG-LP, respectively.

2.5.2. Preparation of PEG-LPs for biodistribution study

Large size as well as small size PEG-LPs composed of EPC and Cholesterol (molar ratio: 7/3) were prepared by following the same process as described above. During film formation, ^{3}H-CHE was added as a nonexchangeable, nonmetabolizable lipid phase marker.

2.5.3. Preparation of PEG-LPs for tumor accumulation study

Large size as well as small size PEG-LPs composed of EPC and Cholesterol (molar ratio: 7/3) were prepared by following the same process as described above. During film formation, 1 mol% rhodamine-DOPE was incorporated to label the lipid composition.

2.5.4. Preparation of DOX loaded PEG-LPs

LPs composed of HSPC: Cholesterol (7:3) were prepared by lipid film hydration method followed by extrusion to control the size. DOX was loaded to the LPs by following the ammonium sulfate gradient method [41,42]. Five mol% PEG or RGD-PEG was added to prepare PEG-LPs (DOX) or RGD-PEG-LPs (DOX), respectively (details are given in Supplementary Data).

2.6. Characterization of PEG-LPs

The mean size and zeta potential of the prepared PEG-LPs were determined using a Zetasizer Nano ZS ZEN3600 instrument (Malvern Instruments Ltd., Worchestershire, UK).

2.7. Cellular uptake of small and large size PEG-LPs

To investigate the cellular uptake of the different size PEG-LPs, 100000 HUVEC cells were seeded on a 35-mm glass-bottom dish (Iwaki, Chiba, Japan) in 2 ml of culture medium for 24 h. The next day, the cells were washed with PBS and incubated with PEG-LPs (100 nmol lipid/2 ml) in Kreb's buffer for 2 h at 37 °C. After 1.5 h of incubation, 5 μl of Hoechst 33342 (1 mg/ml) (Dojindo) was added to stain the nuclei and the suspension was reincubated for an additional 30 min. The medium was then removed followed by washing with PBS. Finally, 1 ml of Krebs buffer was added and the cells were observed by confocal laser scanning microscopy, CLSM (Nikon A1, Nikon Instruments Inc., Tokyo, Japan). The total number of pixel of

internalized PEG-LPs in each confocal image was calculated by using ImagePro-plus software (Media Cybernetics Inc., Bethesda, MD, USA).

2.8. Evaluation of binding constant

To determine the binding constant (Kd value), the cellular uptake of the prepared RGD-PEG-LPs was measured. HUVEC (40,000 cells/well) were seeded on 24-well plates. The next day, the cells were incubated with 500 μl of media consisting 5, 10, 50, 100, 150, 200 μl of LP and remaining part of the Kreb's buffer for 2 h at 37 °C. Finally, the cell supernatant was collected by centrifugation at 12,000 rpm, 4 °C for 5 min and fluorescence intensity was measured (550 nm-590 nm). Number of particles was calculated based on the size and lipid dose of the RGD-PEG-LPs [43–45]. Sigma-plot 12.0 (Systat Software, San Jose, CA, USA) was used to calculate the binding constant (Kd) and maximum binding (Bmax) values for small and large size RGD-PEG-LPs.

2.9. Inhibition of cellular uptake of the RGD-PEG-LPs by free RGD

To examine the effect of excess amount of free peptides on the cellular uptake of different size RGD-PEG-LPs, a cellular uptake experiment was performed in the presence of different concentration of free RGD peptide. HUVEC cells were seeded on a 35-mm glass-bottom dish. Excess RGD peptide (fold v.s. RGD peptide present on the surface of RGD-PEG-LPs used) in Kreb's buffer were added to the prepared glass-bottom dish and incubated for 5 min at 37 °C in an atmosphere of 5% CO_2 and 95% humidity. After 5 min, RGD-PEG-LPs were added and incubated for next 20 min at 37 °C. The cells were washed 3 times with phosphate buffered saline (PBS). Finally, Kreb's buffer was added to each dish followed by CLSM observations.

2.10. Biodistribution of PEG-LPs in tumor-bearing mice

OSRC-2 cells were inoculated on the back of BALB/c nude mice. At a tumor volume of 200–250 mm^3, mice were injected by tail vein with ^{3}H-CHE-labeled PEG-LPs (0.5 μmol lipid/200 μl). At 24 h after injection, blood and other organs were collected and radioactivity was measured (details are given in Supplementary Data).

2.11. In vivo targeting of PEG-LPs to tumor vasculature

At a tumor volume of 100 mm^3, mice bearing OSRC-2 tumor were injected with rhodamine-labeled PEG-LPs (0.5 μmol lipid/200 μl). At 6 h after injection, animals were anesthetized and tumors were collected, followed by immunostaining with FITC-conjugated griffonia simplicifolia isolectin B4 (GS-IB4-FITC) (Vector Laboratories Inc.) for TECs and with Hoechest 33342 for nuclei followed by CLSM analysis.

2.12. In vivo anti-tumor efficacy

DOX loaded PEG-LPs were injected to OSRC-2 tumor (~150 mm^3) bearing mice ($n = 4–5$) with once daily dose of 1.5 mg DOX/kg body weight or with PBS (control) for the first three days (total of 3 injections). Body weights and tumor volumes were recorded at three days intervals. Tumor volume was calculated using the formula: $1/2 \times a \times b^2$, where a and b represent the largest and smallest diameters of tumors, respectively. A slope of tumor volume–time curve, representing the growth rate, of each tumor in the treatment group (T) was calculated and divided by that in the control group (C) to give an index (T/C) for the *in vivo* therapeutic effect, as reported before [46].

2.13. Detection of cell apoptosis

Mice bearing OSRC-2 tumor (~100 mm^3) were injected with once daily dose of 1.5 mg DOX/kg body weight ($n = 3$) for the first three days. At day 4, 200 μl of Apo-Trace solution (Sigma–Aldrich Inc.) was injected via tail vein and incubated for 1.5 h. Mice were anesthetized, tumors and other organs were collected followed by incubation with Alexa Fluor 647-Isolectin (GS-IB4) solution (Invitrogen) to stain the blood vessels followed by CLSM analysis. The total number of pixels of apoptotic cells (green) in each confocal image of the collected organs was calculated by using ImagePro-plus software.

2.14. Anti-angiogenic effect of PEG-LPs (DOX)

Similar dosing of DOX as above was followed for the first three days. At day 4, animals were anesthetized, tumors and other organs were collected, followed by immunostaining with FITC-isolectin for blood vessels and with Hoechest 33342 for nuclei. Anti-angiogenic effect of PEG-LPs was observed under CLSM. The total number of pixel of blood vessel (green) as well as of cell nuclei (blue) in each confocal image of the collected organs were calculated by using ImagePro-plus software.

2.15. Cytotoxicity assay

The sensitivity of OSRC-2 (RCC) and OSRC-EC (TEC) cells to DOX was determined by the *in vitro* WST [2-(2-methoxy-4-nitrophenyl)-3-(4-nitrophenyl)-5-(2,4-disulfophenyl)-2H-tetrazolium, monosodium salt] assay protocol. Briefly, 5000 cells were plated in 96-well plates and incubated overnight. The next day, the cells were exposed to different concentrations of free DOX at 37 °C for 8 h, followed by reincubation for 16 h in the presence of fresh media. The cells were washed with PBS and re-incubated with cell counting kit-8 (CCK-8) solution (Dojindo) for 2 h and absorbance was measured at 450 nm using a microplate reader (Thermo Fisher Scientific Inc.). To measure DOX uptake, 40,000 cells were seeded in 24-well plates and allowed to stand overnight. The next day, the cells were exposed to free DOX (10 μg/ml) at 37 °C for 8 h, followed by washing with PBS. The cell supernatant was collected by centrifuging at 12,000 rpm, 4 °C for 5 min and fluorescence intensity was measured (450 nm–590 nm).

2.16. Toxicological study

Mice bearing OSRC-2 tumor (~100 mm^3) were injected with once daily dose of 1.5 mg DOX/kg body weight ($n = 3$) for the first three days. At day 4, animals were anesthetized and blood samples were drawn and allowed to stand at 4 °C for coagulation. Serum was collected by centrifuging the coagulated blood at 10,000 rpm at 4 °C for 10 min. Serum alanine transaminase (ALT) and aspartate amino transferase (AST) enzyme levels were determined using a commercially available kit (Wako) by following the manufacturer's instructions.

2.17. Statistical analysis

Comparisons between multiple treatments were made using the one-way analysis of variance (ANOVA), followed by the Dunnett test. Pair-wise comparisons of subgroups were made using the student's t-test. Differences among means were considered to be statistically significant at a P value of <0.01 and <0.05.

3. Results

3.1. Characterization of LPs

Liposomes composed of EPC (or HSPC) and cholesterol (7:3) were prepared by the lipid film hydration method followed by extrusion to control the size. The average diameter of small and large size PEG-LPs was determined to be ~120 nm and ~330 nm respectively, with a narrow size distribution and comparable surface charge (Fig. 1A, Table 1). The encapsulation efficiencies of DOX in the small size PEG-LP, the small size RGD-PEG-LP and the large size RGD-PEG-LP were determined to be 98%, 97% and 96% respectively. Similar physical properties as above were found for DOX loaded PEG-LPs (Table S1).

3.2. Size dependent binding of RGD-PEG-LPs to endothelial cells

To observe the effect of size on the cellular association of PEG-LPs, *in vitro* cellular uptake was measured at 37 °C in HUVEC which express remarkable levels of Integrin αvβ3 [22]. Based on qualitative and quantitative analyses, the signals detected from small and large size PEG-LP (Fig. 1B–C) were negligible, indicating that only an increase in the size of PEG-LP does not result in an enhancement in cellular uptake. On the other hand, the small size RGD-PEG-LP showed a greater extent of cellular uptake and a further enhancement was observed for the large size RGD-PEG-LP (Fig. 1B–C).

Based on these results, we next quantitatively determined the binding constant (Kd) for the small and large size RGD-PEG-LPs at 4 °C and 37 °C in HUVEC. Compared to small size, large size RGD-PEG-LP showed about a 10 times higher rate of binding and cellular uptake efficiency (Fig. 1D, Table 1). This was also tested by determining the inhibition of cellular uptake of RGD-PEG-LPs using free RGD (Fig. 1E). Compared to large size, the cellular uptake of small size RGD-PEG-LP was more rapidly inhibited by free RGD; indicating that, compared to small size, large size RGD-PEG-LP caused higher multivalent interactions with Integrin αvβ3 which

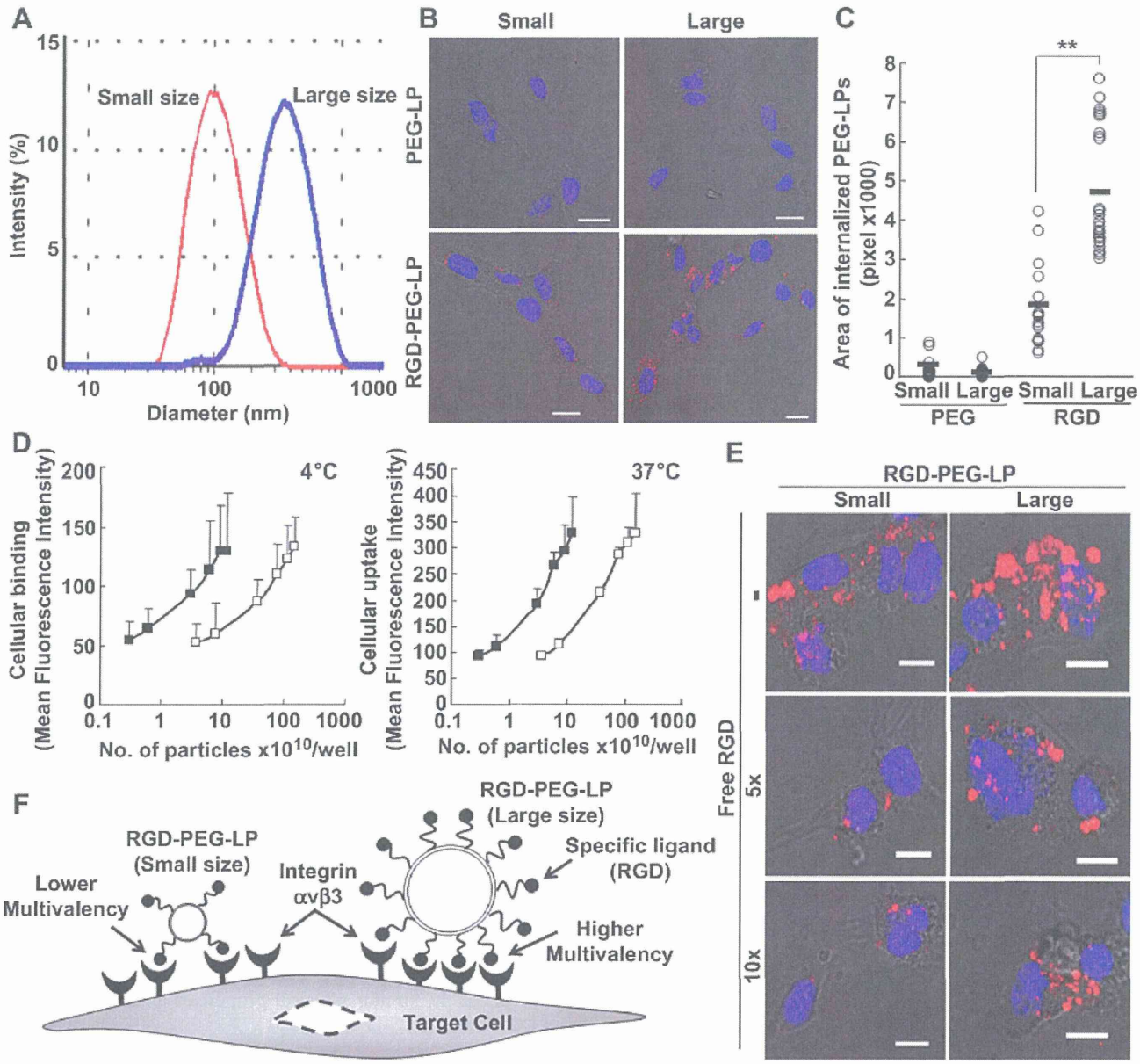

Fig. 1. Size dependent cellular uptake of PEG-LPs in HUVEC. Small and large size PEG-LPs were prepared by lipid film hydration method followed by extrusion to control the size. Size distribution of PEG-LPs was obtained by the DLS measurement (A). Forty thousand cells were incubated with rhodamine labeled PEG-LPs for 2 h at 37 °C and observed under CLSM (B). Area of internalized PEG-LPs (C), as counted from 100, 90, 97 and 105 cells treated with small size PEG, small size RGD, large size PEG and large size RGD, respectively (in at least 15 images/group). Cellular uptake based on the binding of RGD-PEG-LPs to Integrin αvβ3 receptor expressed by HUVEC following a 2 h incubation at 4 °C and 37 °C (D); small size RGD-PEG-LP (square, open), large size RGD-PEG-LP (square, close), mean ± SD, $n = 3–4$. Statistical analysis was done by unpaired t-test (**$P < 0.01$). Inhibition of cellular uptake of RGD-PEG-LPs in presence of free RGD (E). Twenty five thousand cells were incubated with different concentrations of free RGD for 5 min at 37 °C followed by incubation with rhodamine labeled RGD-PEG-LPs for 20 min at 37 °C and observed under CLSM. Blue: DAPI, scale bars 20 μm. Schematic representations of the multivalent interactions of RGD molecules with its target receptor (F), where RGD is present on the top of PEG of either small or large size PEG-LP. (For interpretation of the references to color in this figure legend, the reader is referred to the web version of this article.)

facilitates its prompt internalization (Fig. 1F). These results suggest that large size particles might have the preference to target the diseased tissues.

3.3. Distribution of PEG-LPs in tumor tissues

Based on the above results, we next applied the PEG-LPs to mice bearing OSRC-2 (RCC) tumor. To examine the localization of PEG-LPs within the tumor tissue, mice were injected with [^{3}H]CHE labeled PEG-LPs. Higher amounts of small size PEG-LP were found in the tumor via the EPR effect due to its long circulation property mediated by PEGylation (Fig. 2A). However, the tumor accumulation of large size PEG-LP was lower, which can be attributed to the entrapment of the particles in the splenic filter (Fig. S1A) and possibly from escaping the EPR effect, as indicated by the size dependent distribution of PEG-LPs (Fig. S1B). On the contrary, a similar pattern of accumulation of both small and large size RGD-PEG-LPs was observed in tumors (Fig. 2A) and other tissues (Fig. S1A), indicating its ligand dependent distribution (Fig. S1B). Compared to large size PEG-LP, the tumor accumulation of large size RGD-PEG-LP was found to be higher (Fig. 2A), suggesting that it likely targets the tumor vasculature.

Table 1
Physical properties of size controlled PEG-LPs prepared using EPC, cholesterol as lipid components. The data are expressed as the mean ± SD value from at least six different preparations. Size dependent binding of RGD-PEG-LPs with Integrin αvβ3 receptor expressing from HUVEC. Different lipid doses of RGD-PEG-LPs was added to 40,000 cells and incubated for 2 h at 4 °C and 37 °C. Kd and Bmax values were calculated using the Sigma-plot software. The results expressed as the mean ± SD, $n = 3–4$.

Sample ID		Diameter (nm)	Poly dispersity index (PDI)	Zeta-potential (mV)	Binding constant (Kd value); (no. of particles × 10^{10}/well)		Binding maximum (Bmax); (maximum fluorescence intensity)	
					4 °C	37 °C	4 °C	37 °C
Small size	PEG-LP	121 ± 10	0.12 ± 0.00	−12 ± 7	–	–	–	–
	RGD-PEG-LP	127 ± 2	0.13 ± 0.01	−19 ± 3	2.46 ± 0.39	6.96 ± 2.68	79.4 ± 31.5	223.2 ± 42.7
Large size	PEG-LP	327 ± 8	0.20 ± 0.06	−13 ± 5	–	–	–	–
	RGD-PEG-LP	326 ± 11	0.19 ± 0.03	−16 ± 8	0.25 ± 0.11	0.62 ± 0.52	92.4 ± 21.1	203.3 ± 51.8
Relative binding efficiency of large size RGD-PEG-LP (vs small size)					9.70 ± 2.8	11.2 ± 6.0	–	–

3.4. Association of PEG-LPs to tumor vasculature

Tumor vasculature targeting efficiency was investigated by injecting mice with rhodamine labeled-PEG-LPs. Based on CLSM analyses, a huge amount of small size PEG-LP was found throughout the tumors, indicating that it extravasated and accumulated in the tumor via the EPR effect (Fig. 2B, Fig. S2). However, only a very small amount of large size PEG-LPs was detected in the tumor, which can be attributed to its lower rate of extravasation through the tumor vasculature. On the other hand, the accumulation of small size RGD-PEG-LP in tumors was found to be minimal, due to its lower systemic stability as well as its recognition by the spleen (Fig. S1A). However, a larger amount of large size RGD-PEG-LP was detected in tumors where most of the signals had merged and were located within the tumor blood vessels (Fig. 2B, Fig. S2), indicating its higher tumor vasculature targeting efficiency. These results clearly indicate that the large size PEG-LP could minimize the EPR effect and preferentially target the TECs, provided it is modified with the specific ligand RGD.

3.5. Drug-resistant tumor therapy by DOX loaded PEG-LPs

The therapeutic application of the large size particles was observed and compared to that of the small size particles. Mice bearing OSRC-2 tumor were intravenously injected with 1.5 mg DOX in PEG-LPs/kg body weight. Tumor volumes and life span of mice are presented in Fig. 3. Compared to controls, Doxil was essentially ineffective in inhibiting tumor growth (Fig. 3A). Furthermore, small size RGD-PEG-LP (DOX) failed to show an anti-tumor effect. On the other hand, large size RGD-PEG-LP (DOX) surprisingly exerted a significant anti-tumor effect (Fig. 3A) and prolonged the life span of the mice (Fig. 3B). The index for *in vivo* therapeutic effect (T/C) was calculated to compare the efficacy of the PEG-LPs (DOX) (Table S2). The lower T/C value for large RGD-

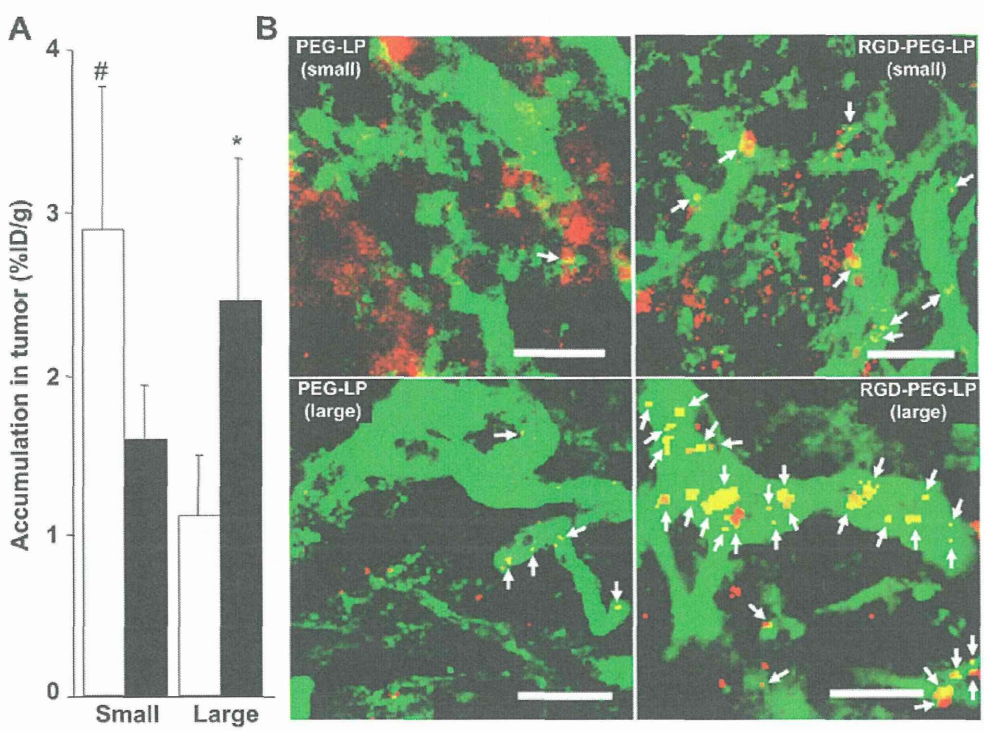

Fig. 2. Distribution of size-controlled PEG-LPs in RCC tumor tissues. Radio-labeled PEG-LPs were injected to mice ($n = 4$) and radioactivity was measured at 24 h post-injection (A); PEG-LPs (□), RGD-PEG-LPs (■). Data presented as mean ± SD. Statistical analyses involved the two-tail unpaired *t*-test. Small PEG vs small RGD #$P < 0.05$; large PEG vs large RGD *$P < 0.05$. Rhodamine labeled PEG-LPs were injected to mice (0.5 μmol lipid/mouse). Representative images of tumors collected at 6 h post-injection are shown (B), green: tumor vessel, blue: DAPI. Small size PEG-LP was detected throughout the tumor, large size RGD-PEG-LP was mostly found along with tumor vessels where it merged (arrows). Scale bars 50 μm. Original images were given in supplementary Fig. S2. (For interpretation of the references to color in this figure legend, the reader is referred to the web version of this article.)

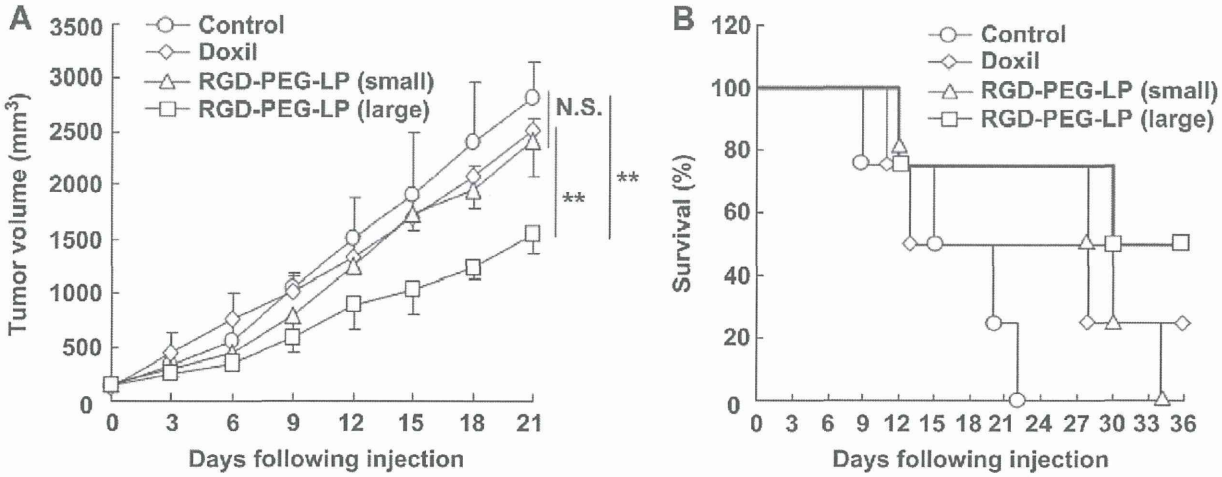

Fig. 3. Therapeutic effect of DOX loaded PEG-LPs in RCC tumor bearing mice. Mice were treated with 1.5 mg/kg DOX in PEG-LPs or with PBS (control). Data presented as mean ± SD ($n = 4–5$). Statistical analysis was done by One-way ANOVA followed by SNK-test. $^{**}P < 0.01$; N.S., not significant.

PEG-LP (DOX) clearly indicates its anti-tumor efficacy as compared to the others.

3.6. Mechanism of the anti-tumor effect

To elucidate the mechanism responsible for the therapeutic action of the PEG-LPs (DOX), the induction of apoptosis within tumors was evaluated (Fig. 4). Compared to controls, almost no apoptotic cells were detected in tumors that had been treated with Doxil (Fig. 4A–B). This result is indicative of the general tendency for RCCs to be resistant to DOX in an *in vivo* situation, which leads to the failure of Doxil to exert an anti-tumor effect. In contrast, a greater amount of apoptotic cells was detected throughout the tumors treated with both small and large size RGD-PEG-LPs (DOX) (Fig. 4A–B); where in tumors treated with small size RGD-PEG-LP (DOX), apoptotic cells were also found both inside and outside the tumor vessels (Fig. 4A), indicating that it can target TECs and can enter tumor cells as well via the EPR effect. However, in the case of large size RGD-PEG-LP (DOX)-treated tumors, most of the apoptotic cells were detected surrounding the tumor vessels (Fig. 4A) where it merged and a greater extent of apoptotic endothelial cells was found, as compared to its small size version (Fig. 4C); indicating that large size RGD-PEG-LP (DOX) largely targets and kills the TECs.

Further, the structure of tumor vessels was observed after injecting the mice with PEG-LPs (DOX). A tumor vessel network was clearly observed in the Doxil treated tumors, similar to the controls (Fig. 4D), indicating that Doxil has no effect on the area of tumor vessels (Fig. 4E) and associated nuclei (Fig. 4F). Small size RGD-PEG-LP (DOX) partially dismantled (Fig. 4D) and reduced the area (Fig. 4E) of tumor vessels, indicating its efficiency for targeting the tumor vasculature, however, no effect on the area of the nuclei was detected (Fig. 4F), indicating that this activity was not sufficient to kill the tumor cells themselves. On the other hand, tumor vessels were clearly destroyed and disappeared in the case of tumors that had been treated with large size RGD-PEG-LP (DOX) (Fig. 4D), and the area of the tumor vessels was significantly reduced (Fig. 4E), indicating that it efficiently targeted the tumor vasculature where it remained attached or internalized into the TECs (Fig. 2B). This is consistent with the significant reduction in the area of nuclei (Fig. 4F) as the result of the passive killing of tumor cells. These results indicate that a lower dose of DOX in large size RGD-PEG-LP is efficient to target and kill TECs as well as to disrupt the tumor vasculature.

3.7. Comparison of the sensitivity of tumor cells and tumor endothelial cells to DOX

To support the remarkable apoptotic effect of large size RGD-PEG-LP (DOX) on the TECs *in vivo* condition, we have evaluated the sensitivity of tumor cells and TECs to DOX. OSRC-ECs were isolated from OSRC-2 tumors as described previously [38–40]. OSRC-2 and OSRC-EC were exposed to different concentrations of free DOX and the sensitivity to DOX was compared. The results showed that OSRC-EC appears to be about 100 times more sensitive to DOX (as evidenced by a 50% reduction in cell viability) compared to OSRC-2 (Fig. 5A), indicating the resistance of OSRC-2 tumor cells to DOX. Even though, at a dose of 10 μg DOX/ml, the amount of DOX in OSRC-2 was found to be 1.5 times higher than that of OSRC-EC (Fig. 5B), OSRC-2 resulted in nearly complete survival. These studies clearly demonstrate that delivering DOX to TECs (OSRC-EC) holds some promise for treating DOX resistant OSRC-2.

3.8. Effect of PEG-LPs (DOX) on normal organs

To observe the effect of DOX loaded PEG-LPs on normal organs, we first evaluated the morphology of blood vessels of the liver, spleen and lung of the OSRC-2 tumor bearing mice. Based on the CLSM analysis, no unusual changes in the blood vessel structures were observed (Fig. 6A). Additionally, as markers for hepatotoxicity, the serum ALT and AST enzyme levels of OSRC-2 mice treated with PEG-LPs (DOX) were also measured (Fig. 6B–C) and no significant difference in these enzymes levels was observed among the treated groups.

4. Discussion

Small size PEG-LPs having ~100 dnm are generally used to target the tumor tissues via the EPR effect [2–4]. We recently reported that the size of LPs has impact on the EPR effect as well as on the targetability of the nanoparticles [37]. In this study, we evaluated the ligand–receptor interaction, drug delivery efficiency and the mechanism of the therapeutic effect as a function of the size of PEG-LPs. The cellular uptake was performed using small size (~100 dnm) and large size (~300 dnm) RGD-PEG-LPs in HUVEC (Fig. 1). Compared to small size, large size RGD-PEG-LP exhibited about a 10 times higher multivalent binding towards its target receptor (Table 1), facilitating the enhancement in cellular association, even though the Bmax values were found to be consistent and temperature dependent. Additionally, the number of RGD

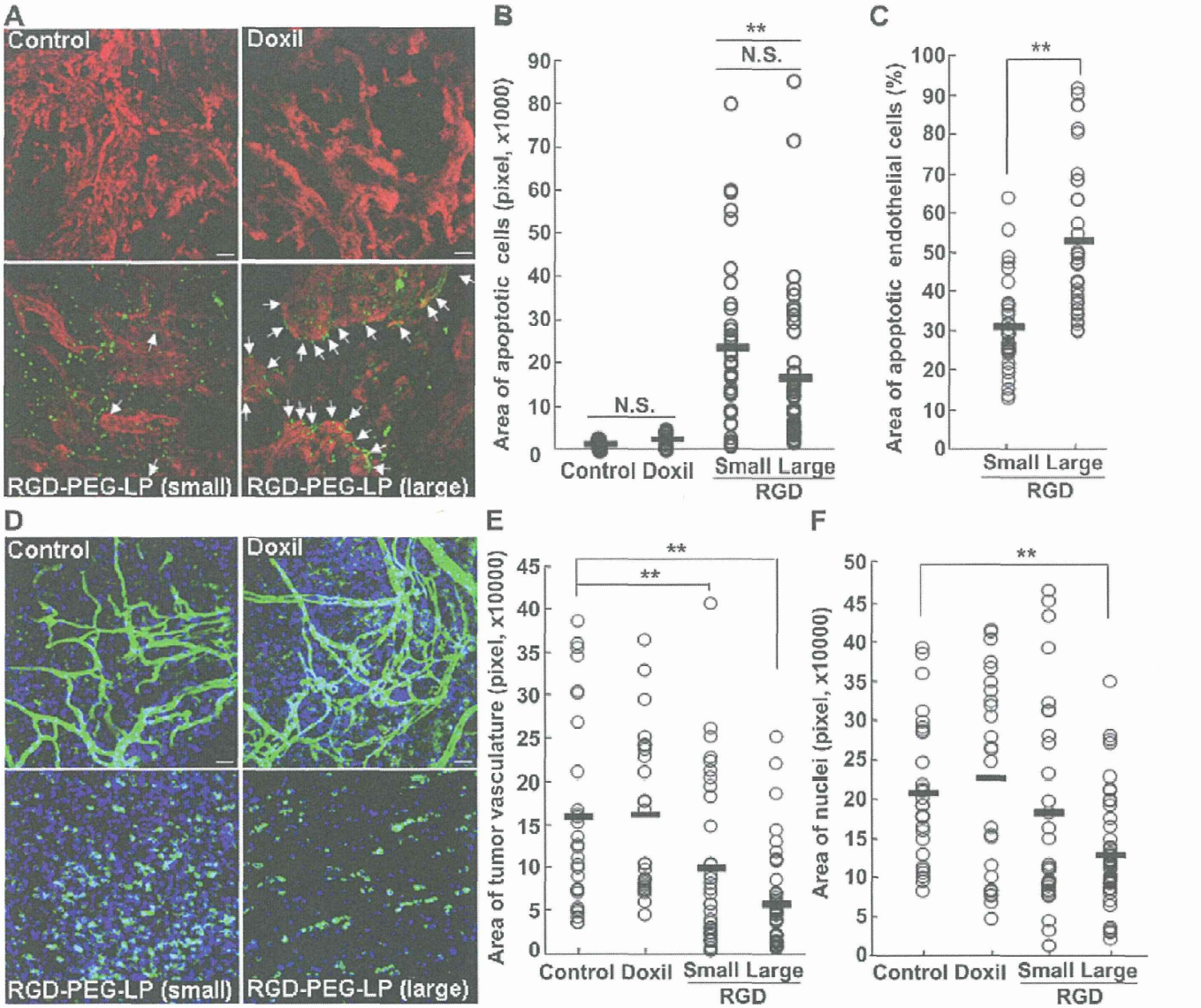

Fig. 4. Site of action and blood vessel disruption effect of DOX loaded size controlled PEG-LPs in tumor. Mice bearing RCC tumors were treated with 1.5 mg/kg DOX ($n = 3$) in PEG-LPs or with PBS. At 24 h post-injection, tumors were collected and analyzed under CLSM. To detect apoptosis in tumors, mice were injected with Apo-Trace solution (A), red: tumor vessel, green: apoptotic cells, arrows: apoptotic endothelial cells. Total area of apoptotic cells (B) and area of apoptotic endothelial cells (C) were counted from at least 35 images taken from different positions in tumors/treated group. Morphology of tumor vessels (D); area of tumor vessel (E), nuclei (F) were counted from 20,758, 19,544, 17,873 and 14,769 cells in 30–50 images taken from different positions of the tumors treated with PBS, DOX loaded small size PEG-LP, small size RGD-PEG-LP and large size RGD-PEG-LP, respectively. Scale bars; 50 μm. Statistical analysis was done by Bonferroni One-way ANOVA followed by SNK-test (B), Dunnett-test (E, F); and unpaired *t*-test (C). $^{*}P < 0.05$; $^{**}P < 0.01$; N.S, not significant. (For interpretation of the references to color in this figure legend, the reader is referred to the web version of this article.)

molecules present on the surface of one large size RGD-PEG-LP was estimated to be ~12.5 times higher than that of the small size version. Therefore, the more rapid cellular internalization of large size RGD-PEG-LP (Fig. 1B) can be attributed to the stronger multivalent binding of the RGD motif to its receptor [47], which finally leads to a higher amount of DOX being delivered to target cells (Fig. S3). These results indicated that large size particles have better preference to target the diseased tissues.

We, next evaluated the distribution of PEG-LPs in tumor tissue. In an *in vivo* situation, the distribution of PEG-LPs in tumor bearing mice was found to be size dependent, where as RGD-PEG-LPs directed a ligand dependent distribution (Fig. 2, Fig. S1). Based on the confocal microscopic analysis, a huge amount of small size PEG-LP was detected in the tumor tissue where it accumulates through the extravasation of the leaky vasculature of RCC tumors (Fig. 2B), a process known as the EPR effect. On the other hand, the accumulation of large size PEG-LP in tumor tissue was found to be negligible (Fig. 2B), indicating that the particles having a ~300 dnm could not provide the EPR effect. Therefore, minimization of extravasation might lead to larger number of large size PEG-LP to remain in the tumor vasculature once it is modified with RGD (RGD-PEG-LP) that finally facilitates the multivalent binding towards its receptor (Fig. 2B), which is present on the surface of TECs (Fig. 1F). In the case of tumor tissue, the small size RGD-PEG-LPs were found to be located both inside and outside the tumor vasculature (Fig. 2B), where most of the signals of the large size RGD-PEG-LPs were detected along with the tumor vasculature. These results indicate that controlling the size of PEG-LPs governs not only its distribution but also dictates the site-specific delivery within the tumor microenvironment.

Based on the above results, it indicated that RGD ligands present on the surface of large size particles have promising advantages to